Published in final edited form as:
IEEE Trans Neural Syst Rehabil Eng. 2008 August ; 16(4): 336–352. doi:10.1109/TNSRE.2008.926716.

Nonlinear Modeling of Causal Interrelationships in Neuronal Ensembles

Theodoros P. Zanos [Student Member, IEEE][1], **Spiros H. Courellis**[2], **Theodore W. Berger [Senior Member, IEEE]**[2], **Robert E. Hampson**[3], **Sam A. Deadwyler**[3], and **Vasilis Z. Marmarelis [Fellow, IEEE]**[2]

[1] T. P. Zanos is with the Biomedical Engineering Department, Biomimetic Microelectronic Systems-Engineering Resource Center (BMES-ERC), Biomedical Simulations Resource (BMSR), University of Southern California, Los Angeles, CA, 90089 USA (e-mail: zanos@usc.edu)

[2] S. H. Courellis, T. W. Berger, and V. Z. Marmarelis are with the Biomedical Engineering Department, University of Southern California, Los Angeles, CA 90089 USA (e-mail: shc@usc.edu, berger@usc.edu; vzm@usc.edu,)

[3] R. E. Hampson and S. A. Deadwyler are with the Physiology and Pharmacology Department, Wake Forest University, Winston-Salem, NC 27157 USA (e-mail: rhampson@wfubmc.edu; sdeadwyl@wfubmc.edu)

Abstract

The increasing availability of multiunit recordings gives new urgency to the need for effective analysis of "multidimensional" time-series data that are derived from the recorded activity of neuronal ensembles in the form of multiple sequences of action potentials—treated mathematically as point-processes and computationally as spike-trains. Whether in conditions of spontaneous activity or under conditions of external stimulation, the objective is the identification and quantification of possible causal links among the neurons generating the observed binary signals. A multiple-input/multiple-output (MIMO) modeling methodology is presented that can be used to quantify the neuronal dynamics of causal interrelationships in neuronal ensembles using spike-train data recorded from individual neurons. These causal interrelationships are modeled as transformations of spike-trains recorded from a set of neurons designated as the "inputs" into spike-trains recorded from another set of neurons designated as the "outputs." The MIMO model is composed of a set of multiinput/single-output (MISO) modules, one for each output. Each module is the cascade of a MISO Volterra model and a threshold operator generating the output spikes. The Laguerre expansion approach is used to estimate the Volterra kernels of each MISO module from the respective input–output data using the least-squares method. The predictive performance of the model is evaluated with the use of the receiver operating characteristic (ROC) curve, from which the optimum threshold is also selected. The Mann–Whitney statistic is used to select the significant inputs for each output by examining the statistical significance of improvements in the predictive accuracy of the model when the respective inputs is included. Illustrative examples are presented for a simulated system and for an actual application using multiunit data recordings from the hippocampus of a behaving rat.

Color versions of one or more of the figures in this paper are available online at http://ieeexplore.ieee.org.

Index Terms

Functional connectivity; hippocampus; input selection; Laguerre expansion; Mann-Whitney; multielectrode; multiinput; multioutput; nonlinear modeling; point process; receiver operating characteristic (ROC) curves; spikes; volterra series

I. Introduction

Computational methods have been used extensively in neuroscience to enhance our understanding of information processing by the nervous system—i.e., the dynamic transformation of neuronal signals as they flow through neuronal ensembles. Quantitative neurophysiological studies have produced computational models that seek to describe the functional relationships between observed neuronal variables of the system of interest. Since brain states are inherently labile and characterized by a high degree of complexity, issues such as neuronal coupling, neuronal coding, neuronal feedback, functional connectivity (convergence/divergence), and functional integration continue to be studied extensively because they are not yet adequately understood. The development of quantitative functional models is a growing trend in computational neuroscience [1]–[6]. Extensive literature discusses various types of models that summarize large amounts of experimental data, using linear or nonlinear methods, depending on the specific characteristics of the system and the goals of the study. Generally, the development of reliable computational models for neuronal ensembles has been hindered by the intrinsic complexity arising from the fact that neuronal function is nonlinear, dynamic, highly interconnected, and subject to stochastic variations. This task is further complicated by the vast amount of time-series data that is required to represent the activity of a neuronal ensemble and by the many possible interactions among the multiple neuronal units. The recent availability of multiunit data recordings (through multiple electrodes or multielectrode arrays) presents a unique opportunity to tackle this important problem if effective methodologies can be developed for their proper analysis. This provides the motivation for the work presented herein

The proper analysis of multiunit recordings requires efficient methodologies for obtaining multiple-input/multiple-output (MIMO) models in a nonlinear dynamic context. This presents us with the daunting complexity of incorporating all existing nonlinear interactions among the various neuronal units. While parametric models (that utilize differential equations to define specific mechanisms or compartments) may provide important insight into the biophysical and physiological aspects of neuronal systems, they require proper validation and are faced with rapidly growing complexity in scaling up to many inputs and outputs. On the other hand, nonparametric models (that utilize Volterra-type functional expansions) provide a general approach that is data-based and does not require *a priori* model postulates, while it is able to scale up to multiple inputs and outputs rather gracefully. Using broadband experimental data, the nonparametric approach yields data-true models that quantify the nonlinear dynamic manner in which multiple “input” neuronal units interact in order to generate the activity of a causally connected output unit. Although issues of computational complexity still arise for large numbers of inputs and outputs, the nonparametric approach allows the methodical search for the important input interactions in a manner that yields complete, robust and accurate models of manageable complexity.

Although linear methods continue to be used in modeling neuronal systems, the bulk of the applications currently utilize nonlinear methods, because nonlinearities are inherent and essential in most neuronal systems [7], [8]. Nonlinear modeling has been applied successfully to several neuronal systems to date, such as the retina [9]–[12], the auditory cortex [13], [14], the visual cortex [15]–[18], the somatosensory system [19], the motor cortex [20], [21], the

cerebellum [22], and the hippocampus [23]–[25]. At the level of single neurons, much work has been done using multicompartmental models based on biophysical principles. Such models attempt to capture known attributes of neuronal structure and function that have been revealed by electrophysiological investigations. These models typically contain a fair number of unknown parameters that must be adjusted in each particular case on the basis of experimental measurements. The use of these models has shed light on several aspects of neuronal function, such as synaptic transmission and somato-dendritic integration [26], [27]. Although such parametric models are extremely useful (when accurate), they present considerable challenges in a practical context with regard to the task of model structure specification and the requisite complexity to approximate the actual system (trade-off between model fidelity and tractability). The problem of model complexity becomes especially acute when we need to scale up the model to accommodate multiple inputs and outputs. Limiting the model parameters to a tractable number can lead to oversimplification of the actual system dynamics, while increasing the number of parameters can raise the model complexity to an impractical level. The issue of model complexity and fidelity is fundamental for the particular subject of this paper: the modeling of neuronal systems with multiple inputs and outputs. The use of multicompartmental models not only makes the problem very complex computationally, but raises also the risk of misrepresentation, since knowledge about the exact way neurons are interconnected and communicate with each other in a nonlinear context is still limited. Thus, inaccurate representation of this interconnectivity (in structural and functional terms) can lead to invalid modeling results and erroneous conclusions.

As an alternative to parametric modeling, the nonparametric approach of Volterra-type modeling employs a general model form and avoids the treacherous task of model specification —especially in the case of nonlinear and highly interconnected systems. For this reason, it is considered a general methodology for nonlinear modeling of physiological systems that is based on a rigorous mathematical framework and provides a quantitative description of the nonlinear dynamics of the input–output relation in the form of a functional series that contains unknown kernel functions estimated from the data. This nonparametric model has predictive capabilities for arbitrary inputs [5]. The first extension of Volterra-type nonparametric modeling to the case of two inputs was made in the study of motion detection in the fly visual system and of ganglion cells in the catfish retina [11], [12]. This approach was extended to spatio-temporal visual inputs and ganglion cell responses in the frog retina [9], [10] or cortical cells [28]. More recent applications to multiple or spatio-temporal inputs have been reported for several neuronal systems [16], [29]. The aforementioned cases concern systems with continuous inputs and continuous outputs. However, the nonparametric modeling methodology has also been applied to neuronal systems with point-process inputs [30], two inputs [31], multiple inputs and a single output [32], and a MIMO system that is modeled using output-triggered feedback [33]. Note that the input–output data required for the effective estimation of the unknown quantities in nonparametric models (Volterra kernels) must have broad spectral content that endows them with predictive capability for arbitrary inputs and makes their estimation robust in the presence of noise.

The nonparametric approach has its own limitations. For instance, direct physiological interpretation of the nonparametric model is difficult, because this model is not developed on the basis of biophysical principles or existing knowledge about the system internal structure, but constitutes instead a data-based representation of the input–output transformation/mapping. Another limitation is that this general approach may lead to cumbersome models in the case of highly nonlinear systems—a problem that has been addressed to some extent by recent work [5]. Finally, a potential problem with the proposed approach is the utilization of least-squares methods for the estimation of the model parameters (Laguerre coefficients of the Volterra kernel expansions) in the context of point-process outputs, where the binary nature of the output may introduce biases in the kernel estimates under certain circumstances

(elaborated in Section V). Nonetheless, computer simulations (where ground truth is available) indicate that these estimation biases are limited in cases with characteristics similar to our application (as demonstrated by the illustrative example presented in Section III). The obtained models in applications to real systems (where ground truth is not available) can be evaluated on the basis of their predictive performance and can be accepted as reasonable model approximations if such performance is deemed satisfactory. Alternative modeling methodologies for point-processes have been presented in the past [34]–[39] with Brillinger's formulation of the maximum-likelihood estimation problem in the binomial context (for Gaussian variations of the postulated stochastic threshold) deserving special note because it yielded excellent results (in the form of linear input–output models) for real point-process data from three Aplysia neurons [43]. In recent studies, probabilistic formulations of neuronal encoding have led to methodologies utilizing maximum-likelihood techniques [33], [41], [42] and network likelihood models [43] that may offer advantages in certain applications.

This paper presents an extension of the nonparametric modeling approach to the case of multiple inputs and outputs that requires only moderate increase in representational complexity and computational effort. The presented methodology estimates a Volterra model with multiple inputs and a single output (MISO) [32] and appends to this output a threshold-trigger operator that generates the spikes at each recorded output. The validation of this MISO model is based on its predictive performance for arbitrary inputs, which is assessed with the use of receiver operating characteristic (ROC) curves commonly used in detection systems. The statistical significance of this predictive capability is assessed with the use of the Mann–Whitney statistic, which is also used for selecting the inputs that are causally linked to each output (i.e., the relevant inputs that significantly affect it). The resulting MIMO model for multiunit recordings is composed of multiple MISO model modules, one for each output.

The actual data analyzed in this paper are collected in connection with the prospective development of hippocampal neuroprostheses that may emulate the nonlinear dynamics of neuronal transmission between the hippocampal regions of dentate gyrus and CA3 or CA1 [44], or between the CA3 and the CA1 regions that are believed to be involved in the processing of information leading to long-term memory formation [45], [46]. Advances in the development of neural prostheses have been remarkable over recent years, with applications in the auditory system (cochlear implants [47]), visual prostheses [48], the motor cortex [49], and brain-machine interfaces [50]. Implementing such neuroprosthetic devices requires quantitative and reliable representation of the transformations performed by the respective neuronal regions in the form of a biomimetic model. Nonparametric, data-based models with predictive capabilities are excellent candidates for this purpose, since they do not require explicit knowledge of the complex underlying mechanisms or neuronal inter-connectivity and provide sufficient predictive accuracy in a robust and computationally tractable manner. In this application, we use multiunit data from behaving rats that are recorded contemporaneously from several spatially distinct sites at the CA3 and CA1 hippocampal regions, while the rats are performing specific behavioral tasks involving memory. These data are used to model the nonlinear multiunit causal relationship between the CA3 (input region) and the CA1 (output region) during these behavioral tasks.

The paper also discusses the strengths and limitations of the Volterra-type modeling methodology adapted to the case of multiple point-process inputs and outputs recorded via multielectrode arrays. Illustrative results from simulated and real systems are presented to demonstrate the efficacy of the proposed modeling approach. The proposed methodology is presented in the following section and the results are presented in the subsequent section.

II. Methods

The proposed MIMO methodology for deriving nonlinear dynamic models of neuronal multiunit transformations utilizes an array of MISO model modules, as shown in Fig. 1(a).

Each MISO module represents the neural transformation of the Q point-process inputs into the respective point-process output. This is done in two stages [see Fig. 1(b)]: (1) a "nonlinear Volterra transformation" (NVT) of the Q input spike sequences $x_q(n)$, q = 1,2,3,mldr;, Q into an intermediate variable $u_p(n)$ that can be interpreted as the transmembrane potential at the axon hillock of the respective pth output neuron (p = 1,2,3,…, P); and (2) a threshold-trigger (TT) operating on the intermediate variable $u_p(n)$ to generate the spikes (action potentials) of the respective point-process output $y_p(n)$ when the intermediate variable exceeds the specified threshold value T_p.

The NVT stage of each MISO module contains a set of Volterra kernels (characteristic of each input–output mapping) that operate on the Q inputs to generate the intermediate variable $u_p(n)$ according to the following mathematical expression (1) of the continuous multiple-input Volterra model

$$\begin{aligned} u_p(n) &= k_{0y_p} + \sum_{q=1}^{Q}\sum_{m=0}^{M-1} k_{1y_p x_q}(m)x_q(n-m) \\ &+ \sum_{q_1}\sum_{q_2}\sum_{m_1}\sum_{m_2} k_{2y_p x_{q_1} x_{q_2}}(m_1,m_2) \\ &\times x_{q_1}(n-m_1)x_{q_2}(n-m_2) \end{aligned} \tag{1}$$

where k_0, k_1, and $k_2$denote the zeroth-, first-, and second-order kernels, respectively. Higher order kernels may generally exist but are not included in these expressions. At the second stage, the threshold-trigger operator for the respective MISO module $TT_p[u_p(n),T_p]$ is applied on the intermediate variable $u_p(n)$ and generates a spike when the threshold value T_p is exceeded.

A. Kernel Estimation With the Laguerre Expansions Method

To facilitate the estimation of the Volterra kernels in the model of (1) and improve the estimation variance by reducing the number of free parameters, we expand the kernels using the discrete-time Laguerre basis functions [28] as

$$\begin{aligned} k_{1y_p x_q}(m) &= \sum_{l=0}^{L-1} c^{(1)}_{y_p x_q l} L_l(m) \\ k_{2y_p x_{q_1} x_{q_2}}(m_1,m_2) &= \sum_{l_1=0}^{L-1}\sum_{l_2=0}^{L-1} c^{(2)}_{y_p x_{q_1} x_{q_2} l_1 l_2} L_{l_1}(m_1)L_{l_2}(m_2) \end{aligned} \tag{2}$$

where $\{c^{(1)}_{y_p x_q l}, c^{(2)}_{y_p x_{q_1} x_{q_2} l_1 l_2}\}$ are the Laguerre expansion coefficients and $L_l(m)$ are the Laguerre basis functions. Substitution of these kernel expansions into (1) gives rise to the multinomial expression of the modified Volterra model [29]

$$y_p(n)=k_0+\sum_{l=0}^{L-1} c^{(1)}_{y_p x_{q_l}} v_l(n) + \sum_{l_1=0}^{L-1}\sum_{l_2=0}^{L-1} c^{(2)}_{y_p x_{q_1} x_{q_2} l_1 l_2} v_{l_1}(n) v_{l_2}(n) + \text{higher order terms} \quad (3)$$

where $v_i(n)$ denotes the convolution of the ith input with the jth Laguerre basis function. The estimation of the Laguerre expansion coefficients (which are now the unknown parameters of the Volterra model) can be performed in (3) via least-squares methods—i.e., by minimizing the sum of the squared errors of the NVT model prediction, denoted by $u_p(n)$ in the model of (1), relative to the point-process output $y_p(n)$, without involving the TT operator. This approach is expected to yield good estimates of the Laguerre expansion coefficients if the distribution of the prediction errors $[y_p(n) - u_p(n)]$ is approximately Gaussian—otherwise biases may exist in the estimates (see Section V). The aggregate effect of these possible biases is assessed through the performance evaluation of the estimated model utilizing ROC curves. An "optimum" threshold T_p of the TT operator can be selected from the ROC curve, as described below. The estimated Laguerre expansion coefficients are used to reconstruct the estimates of the Volterra kernels according to (2).

The Laguerre basis functions are suitable for kernel expansion because they contain an exponential-decay term that forces them asymptotically to zero, as the kernels of stable natural (nonoscillatory) systems must do to avoid instabilities. This rate of decay is determined by the Laguerre parameter alpha that must be selected properly for each system (based on the data). The exponential term of the rath-order Laguerre basis function is multiplied by an mth-degree polynomial that has m roots (i.e., the mth-order Laguerre basis function has m zero-crossings) —see [28] and references therein. These basis functions have proven to be very efficient for the representation of the kernels of real systems, as suggested originally by Wiener in the 1950s and numerous other prominent investigators over the last 50 years. They have proven their utility in nonlinear modeling of physiological systems (for partial review, see [29]).

The savings in representational and computational complexity achieved by the Laguerre expansion of the kernels are considerable. For instance, for a second-order model of a single-input/single-output system with kernel memory of M lags, the unknown discrete kernel values that must be estimated are: M for k_1 and $M(M+1)/2$ for k_2, after taking into account kernel symmetries—for a total of $(M + 1)(M + 2)/2$ unknown discrete kernel values, where the zeroth-order kernel value is also included [29]. A typical value of 50 lags would require the estimation of a total of 1326 unknown discrete kernel values. Obviously, the computational burden of estimating so many unknown kernel values is immense and would require extremely long input–output data sets to avoid high estimation variance. On the other hand, the use of Laguerre expansions for the estimation of the kernels reduces significantly the number of unknown parameters (expansion coefficients) and makes the computational and representational task tractable. If L Laguerre basis functions are used for this purpose, then the total number of unknown expansion coefficients that must be estimated is $(L + 1)(L + 2)/2$. Experience has shown that a maximum of nine Laguerre basis functions ($L = 9$) is required for adequate representation of the kernels of physiological systems, which corresponds to a maximum total of 55 expansion coefficients. Note that $L = 5$ or even $L = 3$ has been found to be adequate in many actual applications, corresponding to a total of 15 or 6 expansion coefficients, respectively. Considerable advantages in terms of estimation accuracy, input–output data requirements and model complexity result from this significant reduction in the number of estimated parameters [28], [29].

Obviously, the number of free parameters increases rapidly in the MIMO case because of the presence of possible nonlinear interaction terms among the various inputs as they affect the outputs. For instance, a second-order MIMO model with Q inputs and P outputs has a total number of free parameters equal to: $PQ(QL^2 + 3L + 2)/2$, which grows mainly as the square of the product QL (dominant dependence) and is only proportional to P. Thus, for a MIMO model with 10 inputs and 10 outputs ($P = Q = 10$), the total number of free parameters, even for $L = 3$, is 5050. This provides the motivation to screen the various inputs and their interactions regarding the significance of their contributions to the output in order to reduce the total number of free parameters in the model (see the Section II-D below).

B. Selection of Threshold and Evaluation of Model Performance using ROC Curves

The predictive capability of the obtained models is the basis for the quantitative evaluation of their performance. When the output data are discretized continuous signals, the most commonly used measure of prediction error is the mean-square error. However, in the case of point-process outputs (as in this study), the mean-square error is not appropriate due to the binary nature of the output, and the balance between counts of correct and incorrect predictions of output spikes should be used instead. A spike predicted by the model is termed a "true positive" (TP), if it coincides with an actual output spike, or it is termed a "false positive" (FP) otherwise. Since the model prediction depends on the threshold value T_p of the TT operator (which is not estimated through the Laguerre expansion method used for kernel estimation), various values of the threshold are applied upon the continuous NTV model prediction $u_p(n)$and the two performance metrics of true positives fraction (TPF) and false positives fraction (FPF) are computed for each value of the threshold according to the relations

$$\begin{aligned}\text{TPF}&=\frac{(\text{number of TP})}{(\text{number of actual output spikes})}\\ \text{FPF}&=\frac{(\text{number of FP})}{(\text{number of non-}\ \text{spikes events})}.\end{aligned} \tag{4}$$

When we plot the FPF value in the abscissa and the TPF value in the ordinate for each threshold value, we obtain the receiver operating characteristic (ROC) curve that was developed in the 1950s as a tool of assessing the performance of detection systems in the presence of noise. The ROC curve is a graphical representation of the competitive relation between sensitivity (TPF) and specificity (1-FPF) of a binary detector/classifier, as its detection threshold changes. The shape of the ROC curve depicts the detection performance and the Area Under the Curve (AUC) is a quantitative measure of this performance (i.e., the model performance is better over all threshold values when the corresponding AUC value is closer to 1, while the worst performance corresponds to an AUC value of 0.5 when the ROC curve coincides with the diagonal). The threshold value that brings the ROC curve closest to the (0, 1) corner-point is often selected as the "optimum" threshold of the model

$$T_p=T_{\text{popt}}:D(T_p)=\min\left\{(1-TP_{T_p})^2+FP_{T_p}^2\right\}. \tag{5}$$

C. Model Statistics

In order to establish the statistical significance of each estimated MISO model (as the quantitative representation of a causal link between the inputs and the output) in the presence of noise or other sources of stochastic variability in the data, we utilize the Mann–Whitney two-sample statistic [17] that relates to the AUC value of the ROC curve and can be used to test statistically whether a specific model is better than another as a binary predictor.

The Mann–Whitney statistic (MWS) represents the probability θ that a randomly selected sample X_i from the intermediate variable $u_p(n)$ that corresponds to zero output will be less than (or equal to) a randomly selected sample Y_i from the values of $u_p(n)$ that correspond to spikes in the output. Essentially the MWS represents how well these two random variables, X_i and Y_i, are separated. It has been shown that the area under the ROC curve (calculated using the trapezoidal rule) is equivalent to the MWS. The unbiased estimate of the MWS is the average of the samples Ψ

$$\Psi(X_i, Y_i) = \begin{cases} 1 & Y \le X \\ 0 & Y > X \end{cases} \tag{6}$$

formed by all possible pair combinations of the two sets of samples X_i and Y_i in the data record. The MWS is a U-statistic and, according to the theory developed by Hoeffding for U-statistics [17], it follows an asymptotically normal distribution with unbiased estimates of its mean and variance calculated from the data. Therefore, we can use a *t*-test to perform statistical testing of significant differences in performance between two models (e.g., with and without certain model component), using the respective MWS. Specifically, the statistical significance of an estimated model can be tested against the null hypothesis of a random predictor (i.e., no causal input–output relationship).

D. Selection of Significant Inputs

The complexity of the MIMO Volterra model depends on the number of inputs that are causally linked to each output, since the number of required kernels rises dramatically with increasing number of inputs. This is especially true in the presence of high-order nonlinearities (higher order Volterra kernels) that give rise to numerous nonlinear interaction terms (cross kernels) and, consequently, to the number of free parameters that must be estimated (i.e., the Laguerre expansion coefficients). As indicated earlier, for a second-order MIMO Volterra model, the total number of free parameters is: $PQ(QL^2 + 3L + 2)/2$, where Q is the number of inputs and P the number of outputs. Therefore, it is important to select only the necessary inputs for each MISO module to achieve the minimum model complexity. The significant inputs are those causally linked to each specific output and they are selected on the basis of their contribution to the prediction of the output using the respective MWS.

The algorithm that selects the causally-linked inputs to each output, builds successive models with increasing number of inputs and examines whether the inclusion of a specific input (or set of inputs) improves the predictive accuracy of the model in a statistically significant sense. The comparison of the predictive accuracy of two successive models is performed by applying the *t*-test (with $p < 0.01$) on the two MWS values that correspond to the compared models. A complete combinatorial search of all possible pair-wise comparisons can be followed in order to select the causally-linked inputs to each output. In order to keep the number of required pair-wise comparisons manageable in the case of a high number of possible inputs, we propose the following procedure that is more efficient.

1. The MWS of each single-input/single-output model is compared with the MWS of a "random" predictor in order to assess whether the input has statistically significant impact on improving the prediction of the respective output (relative to the "random" predictor that serves as the null hypothesis). The random predictor is a single-input/single-output model with the same input as the tested model but with a statistically independent Poisson output having the same mean firing rate as the output of the tested model. The distribution of theta estimates are calculated for the random predictor under these conditions through Monte Carlo runs and a "cutoff value is

established at the 95% significance level that serves as the threshold for the theta estimate obtained from the actual data. The input is accepted as "statistically significant" at the 95% confidence level when the computed theta estimate is higher than the respective cutoff value. After the significant inputs have been selected for each output, we have an initial set of MISO modules comprising the initial MIMO model.

2. We form all possible pairs of the remaining inputs (that were not selected in step 1) with the selected inputs and examine whether the addition of each pair to each initial MISO model has a statistically significant impact on the predictive ability of the model using the MWS. Theta estimates and their variances are calculated for both cases of the model including a pair of inputs and a model without them and used for a *t*-test with a null hypothesis of equal mean values at a 99% confidence level. This step is done in order to explore any possible modulatory interactions between the initially selected inputs and those that were not deemed significant on their own.

The resulting MISO model contains all inputs that are causally-linked with the specific output either directly (step 1) or through modulatory second-order interactions (step 2). One may continue further to examine higher order interactions, but the process becomes rather burdensome and has only limited value (if one posits that any possible higher order interactions are likely to be among inputs that also exhibit second-order interactions already included in the model). This procedure is repeated for each output of the system. The final MIMO model is comprised of the final set of MISO modules thus constructed. Note that the order of nonlinearity of each final MISO module may be determined after the selection of the relevant inputs through a procedure that examines the statistical significance of improvements in model performance (using the MWS) as we extend the order of nonlinearity.

E. Selection of Model Order and Number of Laguerre Functions

In order to select the model order (degree of nonlinearity) of the system and the number of Laguerre functions, we employ the MWS in a similar way to the input selection algorithm. For the model order selection, we start by comparing the first-order with the second-order model using the respective MWS estimates for the two models and a *t*-test. If the second-order model is selected, then the comparison continues between the second-order and the third-order model, until the predictive performance of the higher order model ceases to improve significantly (based on the *t*-test of the respective MWS). The same procedure is followed in order to select the proper number of Laguerre basis functions. The two procedures should be performed jointly by first increasing the number of basis functions and subsequently increasing the model order, until no significant improvement is observed in the respective MWS.

III. Computer-Simulated Example

In order to illustrate the efficacy of the proposed modeling methodology and its robustness in the presence of noise (spurious spikes) and jitter (small shift of spike location) in the input–output data, we consider a second-order MISO system with four independent inputs and a single output (since each output is treated separately as a MISO module in the proposed MIMO approach—see Fig. 1). The functional characteristics of this system are defined by the first-order and second-order Volterra kernels shown in Fig. 2(a) that describe the quantitative manner in which each input affects the output. The form of these kernels resembles the ones that have been experimentally observed. Specifically, the first and second input have first-order excitatory and second-order inhibitory impact on the output, respectively, and the fourth input has the reverse effect; while the third input has no impact on the output since all kernels that link it to the output are zero. A cross-kernel that describes the second-order dynamic interactions between the first and the fourth input as they affect the output is also present (these

are the only existing nonlinear interactions among different inputs in this system). The system is simulated for independent Poisson process inputs with different values of the Poisson parameter λ that defines the mean firing rate of each input.

Since the main application of our modeling methodology involves spike transformations in the hippocampus, we select the mean firing rates of the four inputs to correspond to the average level of activity of four types of hippocampal neurons observed in our experiments (viz. 3 spikes/s, 10 spikes/s, 5 spikes/s, and 1 spikes/s for the first, second, third, and fourth input, respectively). The memory of this simulated system is set at 1 s that corresponds to the observed average memory extent of hippocampal neurons. We select a sampling interval (binwidth) of 10 ms which is slightly smaller than the minimum interspike interval observed in the data and larger than the refractory period; thus, each kernel dimension has 100 sampled values (bins). To estimate the kernels and apply the proposed input-selection method, we use 6000 samples of input–output data that correspond to 1 min of recorded neuronal activity. The threshold of the simulated system is chosen to be 0.22 in order to produce an output mean firing rate of about 12 spikes/s that is consistent with our experimental observations. Validation of the proposed approach is based on the form of the obtained kernel estimates, the input selection and the predictive capability of the model for these input–output data ("in-sample" training set) and an independent set of input–output data ("out-of-sample" testing set). Note that through 500 Monte Carlo simulations of random predictors using the same firing rates and length of data records, we derive a 95% confidence cutoff value to be used as the threshold of significance for each input.

A. Noise-Free Case

First, we test the proposed methodology in the noise-free case (i.e., the input–output data have no spurious spikes). The results of our input selection algorithm are shown in Table I for the testing data sets. The calculated MWS theta estimates for each of the single-input/single-output models are shown in the same Table I, along with the 95% confidence cutoff value from the "random predictor." The resulting decisions of the algorithm are all correct regarding the statistical significance of each specific input in terms of its causal effects on the output.

After the input selection is completed, we determine the proper model order and number L of Laguerre basis functions using a similar MWS-based procedure, as described in Section II. Then, we estimate the Volterra kernels for the selected second-order model using the training data set. The estimated kernels for this simulated example are shown in Fig. 2(b) and exhibit close resemblance to the true kernels. Note that all other cross-kernels (except for the existing $k_{1,4}$) do not contribute to a statistically significant improvement in output prediction when included in the model. Using the estimated kernels, we predict the output of the system for various threshold values of the TT operator and form the ROC curves that are shown in the right compartment of Fig. 2(b) for the training (in-sample) and testing (out-of-sample) data sets. These ROC curves and the corresponding theta values demonstrate the quality of model performance achieved with the proposed methodology.

B. Noisy Case

We now test the proposed methodology in the presence of spurious spikes (noise) in the input–output data. The spurious spikes are independent Poisson processes that are inserted into the noise-free data (all inputs and output). The resulting "noisy" data are analyzed with the previously described algorithms for input selection and kernel estimation. We examined two levels of noise (numbers of inserted spurious spikes): one equal to one-fourth of the total spikes of each input/output process (for example a spike sequence with 100 true spikes will be contaminated with 25 spurious spikes, leading to a total of 125 spikes) and the other equal to half of the total spikes of each input/output process. For the first case (25% added spurious

spikes), the results of the input selection algorithm are shown in Table II and they are not affected adversely. The same is true for the obtained kernel estimates (not shown in the interest of space).

For the second case (50% added spurious spikes), we have the results of input selection shown in Table III. After the input selection, we estimate the Volterra kernels using the noisy input–output data and the results are shown in Fig. 3(a). It is evident that the kernel estimates remain satisfactory, in spite of the large number of spurious spikes, demonstrating the remarkable robustness of this approach even in the presence of a very large number of spurious spikes. Subsequently, we compute the model prediction of the output using the estimated kernels for both training and testing data sets and evaluate its performance using the ROC curves shown on the right of Fig. 3(a) for the "in-sample" and "out-of-sample" cases.

C. Spike Jitter Case

We now test the proposed methodology for the case of random jitter in the location of the input–output spikes that is simulated by introducing stochastic latencies to each one of the spikes, using a normally distributed latency with a mean value of zero and a standard deviation of two lags of jitter. The results of input selection are shown in the Table IV and the estimated kernels with the corresponding ROC curves are shown in Fig. 3(b). These results demonstrate the remarkable robustness of this approach in the presence of spike jitter.

D. Deleted Spikes Case

We also test the proposed methodology for the case where some spikes are mistakenly deleted in the input/output data. In the test performed here, we delete randomly 30% of the total spikes in all inputs and output. The results of input selection are shown in Table V and they are not affected adversely. The same is true for the obtained kernel estimates (not shown in the interest of space).

E. Misassigned Spikes Case

We finally test the proposed methodology for the case where there are misassigned spikes between the four inputs of the model. In the test performed here, we misassign randomly 5% of the total spikes in each input. The results of input selection are shown in Table VI and they are not affected adversely. The same is true for the obtained kernel estimates (not shown in the interest of space).

F. Selection of Model Order and Number of Laguerre Functions

As an illustrative example of the selection procedure for the model order and the number of Laguerre functions that we described earlier, we use the case of 25% spurious spikes case to test the proposed model-order selection algorithm by increasing the model order successively from first to second and then to third for the correct $L = 3$. For each model order, we calculate the MWS theta estimates and run a t-test for the significance of the effect of each model order increase on the output prediction. The results are shown in Table VII and yield the correct answer of a second-order model.

We also test the selection algorithm for the number of Laguerre functions by increasing successively the number of basis functions from two to three and then four (for a second-order model), using the same MWS-based approach as with the model-order selection. The results are shown in Table VIII and yield the correct answer of $L = 3$. In practice, these two searches should be performed together by incrementing L for each model order until a "No" outcome occurs and then incrementing the model order until another "No" outcome occurs.

IV Application to Hippocampal Data

This application is motivated by the development efforts of a hippocampal prosthesis that emulates the multiunit transformations of neuronal activity between different regions of the hippocampus. In this study, we use multiunit data from behaving rats that are recorded contemporaneously from several spatially distinct sites at the CA3 and CA1 hippocampal regions, while the rats are performing a behavioral task involving memory. These data are used to model the nonlinear multiunit functional relationship between the CA3 (input region) and the CA1 (output region) during these behavioral tasks.

Male Long-Evans rats ($n = 11$, 3–11 months of age) were trained on a two-lever spatial delayed-nonmatch-to-sample (DNMS) task with randomly occurring variable delay intervals of 1–40 s [see Fig. 4(a)]. The animal performs the task by pressing the lever presented in the sample phase (left or right) [see Fig. 4(a)(I)]. This constitutes the sample/position information on the trial. The lever is then retracted, and the delay phase initiated, during which the animal must poke its nose into a lighted device on the opposite wall for the duration of the delay [see Fig. 4(a)(II)]. Following the termination of the delay, both levers are extended, and the animal must press the lever opposite the sample/position information [nonmatch response (NR)] [see Fig. 4(a)(III)]. The longer the delay between trials, the less likely it is that the animal to have the correct response on that trial. Correct responses are rewarded with a drop of water delivered to the trough between both levers during a 10 s intertrial interval (ITI). Incorrect responses produce a darkened chamber for 5 s without reward, followed by a 5 s ITI. The next trial is always initiated after at least a 5 s ITI. Only data from correct-response trials were utilized in this study.

To acquire the multiunit recordings, multielectrode arrays of 16 microwires (40 μm) were surgically implanted using both stereotaxic coordinates and spontaneous cell firing activity to position correctly the electrode tips in both the CA3 and CA1 cell layers [Fig. 4(b)]. All arrays had a fixed geometry with 200 μm between pairs (septotemporal axis) and 800 μm between rows (medial-lateral axis) supplied by NB Labs (Denison, TX). Electrode tip length was precisely trimmed to follow the longitudinal curvature of the hippocampus. Data were collected from 11 animals and a total of 198 pyramidal cells (average 16–20 simultaneously recorded per animal) over at least seven DNMS sessions with stable extracellular action potential waveforms and consistent event-specific firing patterns. Neurons that exhibited low firing rates (<0.2 spikes/s) were excluded as unresponsive and neurons with high firing rates (>6 spikes/s) were also excluded as interneurons. Finally, the sampling interval during data acquisition was very small (less than 1 ms), the time binwidth used for the processing of the data was 10 ms, a value smaller than the minimum inter-spike interval of the data analyzed and larger than the refractory period. This binwidth was considered the proper choice for modeling efficiency in this application (i.e., it minimizes the number of sample points while retaining all useful information in the data).

Several instances of each behavioral task were considered across a number of different trials, and all trials were recorded from a specific animal during one session (day) of experiments. Each instance of a behavioral task included the neuronal activity within ±1.5 s around the time of pressing the lever that is associated with the task. Recorded cells from the CA1 area were considered as outputs of the MIMO model, while the CA3 cells contributing to the activity of each output CA1 cell were considered as inputs to for the respective MISO module. The multiunit input–output data recorded during each one of the behavioral tasks (left nonmatch, right nonmatch, left sample, right sample) were analyzed with the proposed methodology and second-order Volterra models were obtained for each MISO module, involving first-order and second-order kernel estimates. The input selection algorithm was applied to each MISO module (corresponding to each of the recorded outputs) and the results are summarized for each of the

four behavioral tasks in Table IX. Note that the MWS estimates for all input channels that were not considered significant with regard to a specific output are omitted in the interest of space. Also note that the theta estimate and its variance for the random predictor are the same for a given output channel (based on the firing rate of that specific output channel) regardless of the input channel.

The resulting selection of CA3 input cells for each CA1 output cell and the causal connections between them for each behavioral task are shown in Figs. 5 and 6. The results from the analysis of the data collected during the Left Sample task are presented in detail (for illustrative purposes) in Fig. 5 that shows the ROC curves (with the corresponding theta value) for each output of the model (A), the estimated first-order kernels (B), the estimated second-order self-kernels and cross-kernels (C), the colormap used to depict the second-order kernels (assigning the red color to the maximum value and the blue color to the minimum value of each kernel (D), a schematic of the topology of the identified input–output causal connections (E), and the MIMO model prediction and the actual recorded activity for each output neuron (F). Note that the Volterra kernels of the obtained second-order MISO modules for all these cases were estimated using three Laguerre basis functions ($L = 3$) and the nonlinear interactions between different inputs were represented in each MISO model by the estimated cross-kernels (when statistically significant). The model predictions shown in Fig. 5(f) for all output CA1 units demonstrate the good predictive capability of the obtained MIMO model. We must note that each MIMO model is animal-specific and task-specific.

A closer inspection of Fig. 5 can provide important information about the functional characteristics of the modeled system and the underlying physiology that are quantified by the Volterra kernels. The vast majority of the first-order kernels and many of the second-order kernels for all outputs and inputs of this system depict a facilitatory characteristic (positive values), an observation that can be explained by the fact that we considered only pyramidal CA3 and CA1 cells (excluding any interneu-rons), thus modeling predominantly the monosynaptic connections between CA3 and CA1 cells which are mostly excitatory. The "effective memory" of most input pathways of this system is about 500 ms, since all the values of most first-order and second-order kernels have become negligible before or around a lag of 500 ms. A few kernels retain significant (but not large) values beyond the lag of 500 ms but not beyond a lag of 1000 ms.

For illustrative purposes, let us examine closer the kernels of output 1 (first line of kernels in Fig. 5) that correspond to three significant inputs. The first-order kernels of all three inputs have a similar shape, with positive values in the early lags and relaxing to zero around a lag of 150 ms. The second-order self-kernels for two (first and third) of the three inputs have a slight depressive effect when the two lags are shorter than 150 ms, while the second-order self-kernel of the second input presents a small facilitatory region when both lags are shorter than 100 ms. The second-order cross-kernel between the first and second input is highly asymmetric, revealing the presence of a modulatory effect that the second input has on the way the first input influences the output—but not significantly the other way around. Specifically, this modulatory effect is triphasic: initially depressive (for lags less than 30 ms), then facilitatory (for lags between 30 and 120 ms) and subsequently depressive again (for lags between 120 and 500 ms). The other two cross-kernels are more symmetrical and while the one between the second and third input is clearly facilitatory for short lags (less than 100 ms), the cross-kernel between the first and second inputs is biphasic (initially depressive up to 80 ms lags and excitatory for longer lags). For the second input, the shapes of first-order kernels exhibit a variety of functional characteristics for the four different inputs. The effect of the third input is excitatory, as well as the fourth (with maximum excitation around 50 ms), while the first and second inputs exhibit a biphasic behavior (initially excitatory and subsequently inhibitory) with the first input dynamics being slower than the second. Also noticeable is the fact that the

first-order and second-order kernels for the third and fifth output [which have the same significant inputs as shown by the schematic in Fig. 5(e)] are very similar to each other.

An illustration of the MIMO model predictions and the actual recorded activity of each output neuron for the other three behavioral tasks are shown in Fig. 6. It is evident that the observed bursts of activity in some output neurons are usually predicted correctly, as well as the intermittent activity. Table X reports the significant input channels for each output channel and the respective theta estimates for the four behavioral tasks. These results demonstrate the predictive capability of the obtained models and the efficacy of the proposed approach.

As a final hypothesis test that the final MIMO models capture an existing temporal dependence, we form the null hypothesis for these MIMO models. We generate N randomly generated independent Poisson spike trains (whose rate parameter follows a normal distribution with a fixed mean value r), which have no causal relationship between each other, and randomly pick one of them as the output and the remaining spike trains (N-1) as the inputs of the system. We build the MISO model for each case and estimate the theta values. We repeat the procedure 50 times and get averaged statistics, that are reported in Table XI, for different values of N and r. This test reveals the baseline of the predictor performance of the proposed modeling approach and establishes the causal relationship captured by the aforementioned models.

V. Discussion

The increasing availability of multiunit recordings gives new urgency to the need for effective analysis of such data that are derived from the recorded activity of neuronal ensembles. A general methodological framework has been presented for analyzing the possible causal links among multiunit recordings from neuronal ensembles by modeling them as systems with multiple inputs and outputs. This methodological framework is broadly applicable (because of the minimal assumptions regarding the underlying system structure) and robust in the presence of noise or errors in the data. It is computationally efficient and applicable in a practical context (e.g., it can be effective with relatively short data records). It is also scalable and flexible to an arbitrary number of inputs and outputs.

The use of functional connectivity measures for ascertaining the subset of significant inputs in multiple-input systems has been suggested in the context of brain-machine interfaces [53] and EMG recordings [54]. As noted by both studies, a large number of inputs not only increases the computational burden but also affects the generalization of the model, thus making the model reduction through input selection an important part of the modeling process. Nonlinear measures of dependency [55] include mutual information [56], which quantifies statistical dependencies between two time-series data without any assumption about their respective probability density functions but is only sensitive to static nonlinear dependencies. Nonlinear interdependences [55], phase synchronization from Hilbert transform [57] and phase synchronization from the wavelet transform [58] can also be used to assess the degree of such dependencies and to capture both linear and nonlinear aspects of causality. The main weakness of these methods is the requirement of sufficient (generally large) amounts of data and, secondarily, the significant computational burden that they add to the modeling procedure.

The method proposed in this paper seeks to identify the inputs that are causally-linked to each output and affect significantly the predictive capability of the model (in a statistical sense embodied in the Mann–Whitney statistic). The proposed approach explores all possible second-order interactions among the inputs and exceeds the capabilities of linear approaches, such as cross-correlation, coherence function, Granger causality and partial directed coherence [59] while keeping the problem computationally tractable size and requiring relatively small amounts of experimental data. As shown with the computer-simulated examples (where ground

truth is available), as well as in the application to real hippocampal data, the method succeeds in capturing the causal relationships wherever they are present. The method was also shown with computer simulations to be remarkably robust in the presence of noise (spurious spikes in the inputs and outputs), jitter in the recorded spike location and deleted or misassigned spikes that may occur in actual recordings and represent serious impediments in the use of other methods in actual applications.

Let us recap the fundamental rationale of the proposed modeling approach. We posit the existence of an internal/intermediate continuous variable $u(n)$ that is generated by the inputs being transformed through a multiinput Volterra model (the operator NVT in Fig. 1) operating in discrete time $n = t/Dt$, where Dt denotes the time-binwidth which is selected slightly larger than the effective refractory period of the specific neuron (10 ms in this case). We view this intermediate variable $u(n)$ as representing the transmembrane potential at the axon hillock of the output neuron and we posit further that an output spike is generated if, and only if, this variable exceeds a threshold value T. This threshold value and the parameters of the aforementioned MISO discrete-time Volterra model of the operator NVT must be estimated from the input–output data in this deterministic formulation (using currently the least-squares method). It is evident that this modeling problem is comprised of two critical steps: 1) estimation of the kernels of the NVT model and 2) the selection of the appropriate threshold for the operator TT. The former is currently accomplished via the least-squares method in an approximate manner (see further comments below) and the latter through the use of ROC curves —which also provide the quantitative means for evaluating the model performance.

The use of the Volterra kernels as the basis of the proposed modeling methodology assures excellent predictive capabilities for the timing of output spikes in response to arbitrary inputs and provides reliable quantitative descriptors of the underlying system dynamics—linear and nonlinear—in a manner that advances scientific knowledge and allows the rigorous testing of scientific hypotheses. Application of the proposed methodology to the real hippocampal data has revealed distinct spatio-temporal connectivity patterns between neuronal populations in the CA3 (input) and CA1 (output) region of the rat hippocampus for each of four different behavioral tasks. The false-negatives (misses) that are seen in the output predictions by the model may be due either to the selection of the “optimum” threshold that balances the true-positives with the false-positives, thus resulting to some false-negatives (misses), or to the presence of spurious spikes in the actual output that are not related to the inputs and, therefore, are not predicted by the model. Among these “spurious” spikes there may be spikes due to “spontaneous activity” of the neurons that has been modeled in the past by incorporating in the threshold operator a monotonic function of time independent of the input (see, for instance, [40]). This input-independent function leads to neuron firing even in the absence of input (spontaneous activity). Our model does not currently incorporate such a feature, but it can easily accommodate it as an additive term to the intermediate variable $u(n)$—provided that its form can be reasonably postulated.

There are three known drawbacks of the proposed methodology. The first is model complexity. The obtained MIMO model generally has considerable complexity (many kernels for multiple, nonlinearly interacting inputs). However, the use of Laguerre expansions of the kernels and the input selection algorithm reduce the model complexity significantly and make the modeling problem tractable, requiring only modest computational effort for the ambitious task of MIMO modeling. Nonetheless, the large number of kernels, as shown in Fig. 5, also makes the interpretation of the model difficult and comprehension of the model overwhelming for most investigators. This has provided the motivation for exploring in future studies the use of principal dynamic modes to reduce this model complexity [5]. The second drawback is that our methodology is deterministic in nature and cannot incorporate the stochastic aspects of biological phenomena. One such limitation in the context of the present application is the

inability to incorporate the likely stochastic variations in the spike-triggering threshold. The third drawback is the possible bias introduced in the kernel estimates of the NVT component of each MISO module by the employed least-squares method. Note that the optimality of the least-squares estimation method is guaranteed only when the model prediction errors follow a Gaussian distribution (when it becomes equivalent to the optimal maximum-likelihood estimation). In this application, the model prediction errors are not expected to follow a Gaussian distribution because of the binary nature of the output point-process. Therefore, the least-squares method of estimation is not optimal—i.e., it does not generally yield unbiased estimates with minimum variance. The extent of this estimation bias depends on the specific characteristics of each problem and relates to the issue of the truncation of the Volterra model and its implications for the obtained kernel estimates. The proposed methodology is based on the premise that the resulting estimation bias will generally be small and the obtained kernel estimates will be satisfactory *approximations* of the actual kernels. The validity of this premise can be examined after the model estimation is completed by evaluating the model predictive performance. If the latter is satisfactory, then the validity of this premise can be accepted.

This issue has been examined through computer simulations (where ground truth is available) and, as expected, the answer is that the severity of the estimation bias depends on the particular characteristics of each estimation problem (system structure and threshold statistics). Nonetheless, the results of the computer-simulated example presented in the manuscript (which seek to emulate the kernel forms found in this application), demonstrate that the obtained least-square estimates of the kernels of NVT are very close to the actual kernels used in the simulation. This provides some reassurance that the least-squares estimates of the kernels are likely to be reasonable approximations, but it does not guarantee the extent of possible estimation biases. Because of the potential importance of this issue, we are currently exploring alternative estimation methods that will guarantee unbiased kernel estimates in the case of point-process outputs—including the maximum-likelihood approach using the binomial distribution of the point-process output—akin to the Brillinger' s formulation of the problem in the linear case [40] and iterative estimation methods that avoid estimation biases by employing a cost function consistent with the binary nature of the output.

The proposed input selection method seeks to determine which of the predesignated inputs are statistically significant in terms of their effects of the respective output in the MISO context. The proposed approach does not seek the "minimum set of inputs" in the sense of a maximally reduced model and, therefore, it does not exclude "relay-type" of neurons (i.e., neurons that receive exclusive input from other predesignated input neurons and simply relay it—perhaps transformed—to the output neuron). If one is only interested in the overall input–output mapping, then these "relay-type" neurons can be excluded in the interest of model parsimony. However, the purpose of the proposed approach is simply to determine whether there is a significant causal link between each of the predesignated inputs and the specific output of each MISO model. Nonetheless, the minimum set of inputs can be determined in a subsequent step of analysis whereby one input is excluded on a rotating basis and the effect on the output prediction is assessed statistically (using the MWS) so that this input can be excluded if the effect is insignificant. This problem was addressed in the past through the use of "partial coherence" measures in the linear case [40].

Finally, it must be emphasized that the identified "causal" relationships between input and output variables (point-processes) in a real neuronal system are only temporal statistical dependencies and cannot be fully substantiated as manifestations of causality without further evidence about the internal workings of the system. For instance, the common effect of a "third party" on both input and output may be viewed mistakenly as the result of an input–output causal relationship. An excellent example of this was presented in the aforementioned study of the three *Aplysia* neurons, where two of them were affected by the third in a manner that

gave the false impression of a causal link between them, although none existed as ascertained by use of the "partial coherence" measures [40]. It is important to keep this possibility in mind, although it should not discourage us from seeking the "statistical dependencies" in actual multiunit data, since the latter can provide important insight into the system function when cast in the proper modeling framework.

Acknowledgments

This work was supported in part by the National Science Foundation (NSF) funded Biomimetic Microelectronic Systems-Engineering Resource Center (BMES-ERC) and the in part by the NIH/NIBIB-funded Biomedical Simulations Resource (BMSR).

Biographies

Theodoros P. Zanos (S'00) was born in Drama, Greece, on July 31, 1980. He received the Diploma degree in electrical and computer engineering from the Aristotle University of Thessaloniki, Thessaloniki, Greece, in 2004, and the M.S. degree in biomedical engineering, in 2006, from the University of Southern California, Los Angeles, where he is currently working toward the Ph.D. degree in the Department of Biomedical Engineering.

Since 2004, he has been a Research Assistant at the National Science Foundation (NSF)-funded Biomimetic Microelectronic Systems Engineering Resource Center and the NIH/National Institute of Biomedical Imaging and Bioengineering (NIH/NIBIB)-funded Biomedical Simulation Resource. His main research interests are in the areas of nonlinear system identification and modeling of neural systems, neural prosthesis, nonparametric methods of MIMO systems modeling and spatiotemporal/spectrotemporal modeling of nonlinear systems, with applications to neural information processing.

Mr. Zanos is a student member of Biomedical Engineering Society and Society for Neuroscience.

Spiros H. Courellis was born on June 3, 1962 in Nemea, Greece. He received the electrical and computer engineering Diploma from the Aristotle University of Thessaloniki, Thessaloniki, Greece in the M.S. degree in electrical engineering from the California Institute of Technology, Pasadena, in and the Ph.D. degree in electrical engineering from the University of Southern California, Los Angeles, in 1992.

From 1993 to 2004, he was a Research Associate with the Biomedical Engineering. Department at the University of Southern California. He was also involved in industrial research and design, education, and leadership. Currently, he is a Research Assistant Professor of Biomedical Engineering at the University of Southern California, Los Angeles, and an Assistant Professor of Computer Science at California State University, Fullerton. His main research interests are in the areas of computational modeling of neural systems, biologically inspired information fusion systems, biosensors, neural computation and memory, embedded computing, sensor networks, and distributed implantable secure medical devices.

Dr. Courellis is a member of the ACM and the Society for Neuroscience.

Theodore W. Berger (M'03-SM'04) received the Ph.D. degree from Harvard University, Cambridge, MA, in 1976.

He is the David Packard Professor of Engineering, Professor of Biomedical Engineering and Neuroscience, and Director of the Center for Neural Engineering at the University of Southern California (USC), Los Angeles. He conducted postdoctoral research at the University of California, Irvine, from 1977 to 1978, and was an Alfred P. Sloan Foundation Fellow at The Salk Institute, La Jolla, CA, from 1978 to 1979. He joined the Departments of Neuroscience and Psychiatry at the University of Pittsburgh, Pittsburgh, PA, in 1979, being promoted to Full Professor in 1987. Since 1992, he has been Professor of Biomedical Engineering and Neurobiology at USC, and was appointed the David Packard Chair of Engineering in 2003. In 1997, he became Director of the Center for Neural Engineering, Los Angeles, in 1997, an organization which helps to unite USC faculty with cross-disciplinary interests in neuroscience, engineering, and medicine. He has published many journal articles and book chapters, and is the coeditor of a book recently published by the MIT Press on *Toward Replacement Parts for the Brain: Implantable Biomimetic Electronics as Neural Prostheses.*

Dr. Berger's thesis work received the James McKeen Cattell Award from the New York Academy of Sciences. During that time, he received a McKnight Foundation Scholar Award, twice received an NIMH Research Scientist Development Award, and was elected a Fellow of the American Association for the Advancement of Science. While at USC, Dr. Berger has received an NIMH Senior Scientist Award, was awarded the Lockheed Senior Research Award in 1997, was elected a Fellow of the American Institute for Medical and Biological Engineering in 1998, received a Person of the Year "Impact Award" from the AARP in 2004 for his work on neural prostheses, was a National Academy of Sciences International Scientist Lecturer in 2003, and an IEEE Distinguished Lecturer in 2004—2005. In 2005, he received a "Great Minds, Great Ideas" Award from the *EE Times* in the same year, and in 2006, was awarded USC's Associates Award for Creativity in Research and Scholarship.

Robert E. Hampson received his Ph.D. degree in physiology from Wake Forest University, Winston-Salem, NC, in 1988.

He was a Postdoctoral Fellow and Assistant Professor at Wake Forest University, Winston-Salem, NC, from 1989 to 1998 when he was promoted to the rank of Associate Professor. He is an Associate Professor in the Department of Physiology and Pharmacology, Wake Forest University School of Medicine, Winston-Salem, NC. He is a past member of the IFCN-7 National Institutes of Health (NIH) review panel and has served as an *ad hoc* member of other review panels for NIH. His main interests are in learning and memory, in particular deciphering the neural code utilized by the hippocampus and other related structures to encode behavioral

events and cognitive decisions. His other interests are in linear and nonlinear modeling of neural encoding of cognitive processes as well as alterations of that encoding by drugs of abuse. He has published extensively in the areas of cannabinoid effects on behavior and electrophysiology, and the correlation of behavior with multineuron activity patterns, particularly applying linear discriminant analysis to neural data to decipher population encoding and representation.

Samuel A. Deadwyler received the Ph.D. degree from the State University of New York, Stony Brook, and conducted postdoctoral research at the University of California, Irvine.

He is a Professor with the Department of Physiology and Pharmacology, Wake Forest University School of Medicine (WFUSM), Winston-Salem, NC, where he has been since 1978. He has been funded by the National Institutes of Health (NIH) continuously since 1974. He is on the editorial board of the journal *Hippocampus* and has been an invited Grass Foundation lecturer on several different occasions. He is past president of the International Cannabinoid Research Society and was elected to the Board of Directors of the College on Problems of Drug Dependence for a four-year term. He has published extensively in journal articles, chapters, and books on his research into neural mechanisms of learning and memory as well as cellular neurophysiological investigation of drug actions. His research interests include mechanisms of information encoding in neuronal populations, relationship between neuronal codes and behavioral performance, mechanisms of enhancement of short-term memory in relation to neural codes generated in the hippocampus and frontal cortex. He served on the editorial board for the *Journal of Neuroscience* from 1996 to 2005 during which time he was also a reviewing editor.

Dr. Deadwyler is the recipient of a National Institutes of Health Senior Research Scientist award from 1987 to 2008 and also a MERIT award from 1990 to 2000.

Vasilis Z. Marmarelis (M'79-SM'94-F'97) was born in Mytiline, Greece, on November 16,1949. He received the Diploma degree in electrical engineering and mechanical engineering from the National Technical University of Athens, Athens, Greece, in 1972 and the M.S. and Ph.D. degrees in engineering science (information science and bioinformation systems) from the California Institute of Technology, Pasadena, in 1973 and 1976, respectively.

After two years of postdoctoral work at the California Institute of Technology, he joined the faculty of Biomedical and Electrical Engineering at the University of Southern California, Los Angeles, where he is currently Professor and Director of the Biomedical Simulations Resource, a research center funded by the National Institutes of Health since 1985 and dedicated to

modeling/simulation studies of biomedical systems. He served as Chairman of the Biomedical Engineering Department from 1990 to 1996. His main research interests are in the areas of nonlinear and nonstationary system identification and modeling, with applications to biology and medicine. His other interests include spatio-temporal and MIMO modeling of nonlinear systems, with applications to neural information processing, closed-loop system modeling, and high-resolution 3-D ultrasonic imaging and tissue classification. He is coauthor of *Analysis of Physiological System: The White Noise Approach* (Plenum, 1978; Russian translation: Moscow, Mir Press, 1981; Chinese translation: Academy of Sciences Press, Beijing, 1990), editor of three research volumes on *Advanced Methods of Physiological System Modeling* (Plenum, 1987, 1989, 1994) and author of a monograph on *Nonlinear Dynamic Modeling of Physiological Systems* (IEEE Press and Wiley Interscience, 2004). He has published more than 100 papers and book chapters in the areas of system modeling and signal analysis.

Dr. Marmarelis is a Fellow of the American Institute for Medical and Biological Engineering.

References

1. Stark, L. Neurological Control Systems: Studies in Bioengineering. New York: Plenum; 1968.
2. Marmarelis, PZ.; Marmarelis, VZ. Analysis of Physiological Systems: The White Noise Approach. New York: Plenum; 1978.
3. Koch, C.; Segev, I., editors. Methods in Neuronal Modeling: From Synapses to Networks. Cambridge, MA: MIT Press; 1989.
4. Poznanski, RR., editor. Modeling in the Neurosciences. Amsterdam, The Netherlands: Harwood Academic Publishers; 1999.
5. Marmarelis, VZ. Nonlinear Dynamic Modeling of Physiological Systems. Piscataway, NJ: Wiley-IEEE Press; 2004.
6. Wu MC, David SV, Gallant JL. Complete functional characterization of sensory neurons by system identification. Annu Rev Neurosci 2006;29:477–505. [PubMed: 16776594]
7. Carandini M, Demb JB, Mante V, Tolhurst DJ, Dan Y, Olshausen BA, Gallant JL, Rust NC. Do we know what the early visual system does? J Neurosci 2005;25:10577–10597. [PubMed: 16291931]
8. Ito M, Tamura H, Fujita I, Tanaka K. Size and position invariance of neuronal responses in monkey inferotemporal cortex. J Neurophysiol 1995;73:218–226. [PubMed: 7714567]
9. Citron MC, Kroeker JP, McCann GD. Nonlinear interactions in ganglion cell receptive fields. J Neurophysiol 1981;46:1161–1176. [PubMed: 6275040]
10. Citron MC, Emerson RC, Levick WR. Nonlinear measurement and classification of receptive fields in cat retinal ganglion cells. Ann Biomed Eng 1988;16:65–77. [PubMed: 3408052]
11. Marmarelis PZ, Naka KI. Nonlinear analysis and synthesis of receptive field responses in the catfish retina II: One-Input white-noise analysis. J Neurophys 1973;36:619–633.
12. Marmarelis PZ, Naka KI. Identification of multi-input biological systems. IEEE Trans Biomed Eng Mar;1974 BE-21(2):88–101. [PubMed: 4818804]
13. McAlpine D. Creating a sense of auditory space. J Physiol 2005;566:21–28. [PubMed: 15760940]
14. Young ED, Calhoun BM. Nonlinear modeling of auditory-nerve rate responses to wideband stimuli. J Neurophysiol 2005;94(6):4441–4454. [PubMed: 16162837]

15. Carandini M, Heeger DJ, Movshon JA. Linearity and normalization in simple cells of the macaque primary visual cortex. J Neurosci 1997;17:8621–8644. [PubMed: 9334433]
16. Pack CC, Conway BR, Born RT, Livingstone MS. Spatiotemporal structure of nonlinear subunits in macaque visual cortex. J Neurosci 2006;26(3):893–907. [PubMed: 16421309]
17. Rapela J, Mendel JM, Grzywacz NM. Estimating nonlinear receptive fields from natural images. J Vision 2006;6(4):441–474.
18. Simoncelli EP, Heeger DJ. A model of neuronal responses in visual area MT. Vis Res Mar;1998 38 (5):743–761. [PubMed: 9604103]
19. Lao R, Favorov OV, Lu JP. Nonlinear dynamical properties of a somatosensory cortical model. Inf Sci 2001;132(1–4):53–66.
20. Paninski L, Fellows MR, Hatsopoulos NG, Donoghue JP. Spatiotemporal tuning of motor neurons for hand position and velocity. J Neurophysiol 2004;91:515–532. [PubMed: 13679402]
21. Truccolo W, Eden UT, Fellows MR, Donoghue JP, Brown EN. A point process framework for relating neural spiking activity to spiking history, neural ensemble, and extrinsic covariate effects. J Neurophysiol 2005;93(2):1074–1089. [PubMed: 15356183]
22. Yamazaki T, Tanaka S. The cerebellum as a liquid state machine. Neural Netw 2007;20:290–297. [PubMed: 17517494]
23. Berger TW, Eriksson JL, Ciarolla DA, Sclabassi RJ. Nonlinear systems analysis of the hippocampal perforant path-dentate projection. II. effects of random train stimulation. J Neurophys 1988;60:1077–1094.
24. Berger TW, Baudry M, Brinton RD, Liaw JS, Marmarelis VZ, Park AY, Sheu BJ, Tanguay AR. Brain-implantable biomimetic electronics as the next era in neural prosthetics. Proc IEEE 2001;89:993–1012.
25. Sclabassi RJ, Eriksson JL, Port RL, Robinson GB, Berger TW. Nonlinear systems analysis of the hippocampal perforant path-dentate projection. I. theoretical and interpretational considerations. J Neurophysiol 1988;60:1066–1076. [PubMed: 3171656]
26. Dayan, P.; Abbot, LF. Theoretical Neuroscience, Computational and Mathematical Modeling of Neural Systems. Cambridge, MA: MIT Press; 2005.
27. London M, Hausser M. Dendritic computation. Annu Rev Neurosci 2005;28:503–532. [PubMed: 16033324]
28. Emerson RC, Citron MC, Vaughn WJ, Klein SA. Nonlinear directionally selective subunits in complex cells of the cat striate cortex. J Neurophysiol 1987;58:33–65. [PubMed: 3039079]
29. van Kleef J, James AC, Stange G. A spatiotemporal white noise analysis of photoreceptor responses to UV and green light in the dragonfly median ocellus. J Gen Physiol 2005;126(5):481–497. [PubMed: 16260838]
30. Marmarelis VZ, Berger TW. General methodology for nonlinear modeling of neural systems with poisson point-process inputs. Math Biosci 2005;196:1–13. [PubMed: 15963534]
31. Dimoka A, Courellis SH, Gholmieh G, Marmarelis VZ, Berger TW. Modeling the nonlinear properties of the in vitro hippocampal perforant path-dentate system using multi-electrode array technology. IEEE Trans Biomed Eng Feb;2008 55(2):693–702. [PubMed: 18270006]in press
32. Zanos, TP.; Courellis, SH.; Hampson, RE.; Deadwyler, SA.; Marmarelis, VZ.; Berger, TW. A multi-input modeling approach to quantify hippocampal nonlinear dynamic transformations. Int. Conf. IEEE Eng. Med. Biol. Soc.; New York. 2006. p. 4967-4970.
33. Song D, Chan RHM, Marmarelis VZ, Hampson RE, Deadwyler SA, Berger TW. Nonlinear dynamic modeling of spike train transformation for hippocampal-cortical prostheses. IEEE Trans Biomed Eng Jun;2007 54(6):1053–1065. [PubMed: 17554824]
34. Brillinger DR. The identification of point process systems. Ann Probabil 1975;3:909–924.
35. Brillinger DR, Bryant HL, Segundo JP. Identification of synaptic interactions. Biol Cybern 1976;22:213–228. [PubMed: 953079]
36. Cox, DR.; Lewis, PAW. The Statistical Analysis of Series of Event. London, U.K.: Nethuen; 1966.
37. Snyder, DL. Random Point Processes. New York: Wiley; 1975.

38. Maas W, Natschlager T, Markram H. Real-time computing without stable states: A new framework for neural computation based on perturbations. Neural Comput 2002;14(11):2531–2560. [PubMed: 12433288]
39. Ogata Y, Akaike H. On linear intensity models for mixed doubly stochastic poisson and self-exciting point processes. J Roy Stat Soc Ser B 1982;44:102–107.
40. Brillinger DR. Maximum likelihood approach to the identification of neuronal firing systems. Ann Biomed Eng 16(1):3–16. [PubMed: 3408049]
41. Paninski L, Pillow JW, Simoncelli EP. Maximum likelihood estimation of a stochastic integrate-and-fire neural encoding model. Neural Comput 2004;16(12):2533–2561. [PubMed: 15516273]
42. Truccolo W, Eden UT, Fellows MR, Donoghue JP, Brown EN. A point process framework for relating neural spiking activity to spiking history, neural ensemble and extrinsic covariate effects. J Neurophysiol 2005;93(2):1074–1098. [PubMed: 15356183]
43. Okatan M, Wilson MA, Brown EN. Analyzing functional connectivity using a network likelihood model of ensemble neural spiking activity. Neural Comp 2005;9:1927–1961.
44. Gholmieh G, Courellis SH, Marmarelis VZ, Berger TW. An efficient method for studying short-term plasticity with random impulse train stimuli. J Neurosci Methods 2002;121:111–127. [PubMed: 12468002]
45. Gholmieh G, Courellis SH, Marmarelis VZ, Berger TW. Nonlinear dynamic model of CA1 short-term plasticity using random impulse train stimulation. Ann Biomed Eng 2007;35:847–857. [PubMed: 17380396]
46. Gruart A, Munoz MD, Delgado-Garcia JM. Involvement of the CA3-CA1 synapse in the acquisition of associative learning in behaving mice. J Neurosci 2006;26(4):1077–1087. [PubMed: 16436593]
47. Wilson, B. Cochlear Implant Technology. Philadelphia, PA: Lippin-cott Williams Wilkins; 2000.
48. Weiland JD, Humayun MS. Intraocular retinal prosthesis. IEEE Eng Med Biol Mag 2006;25(1):60–66. [PubMed: 17020200]
49. Schwartz AB, Cui XT, Weber DJ, Moran DW. Brain-controlled interfaces: Movement restoration with neural prosthetics. Neuron 2006;52(1):205–220. [PubMed: 17015237]
50. Lebedev MA, Nicolelis MA. Brain-machine interfaces: Past, present and future. Trends Neurosci Sep;2006 29(9):536–546. [PubMed: 16859758]
51. Marmarelis VZ. Identification of nonlinear biological systems using laguerre expansions of kernels. Ann Biomed Eng 1993;21:573–589. [PubMed: 8116911]
52. Hoeffding W. A class of statistics with asymptotically normal distribution. Ann Math Statist 1948;19 (3):293–325.
53. Sanchez JC, Carmena JM, Lebedev MA, Nicolelis MA, Harris JG, Principe JC. Ascertaining the importance of neurons to develop better brain-machine interfaces. IEEE Trans Biomed Eng Jun;2004 51(6):943–953. [PubMed: 15188862]
54. Westwick DT, Pohlmeyer EA, Solla SA, Miller LE, Perreault EJ. Identification of multiple-input systems with highly coupled inputs: Application to EMG prediction from multiple intracortical electrodes. Neural Comput Feb;2006 18:329–355. [PubMed: 16378517]
55. Quiroga QR, Kraskov A, Kreuz T, Grassberger P. Performance of different synchronization measures in real data: A case study on electroencephalographic signals. Phys Rev E 2002;65:041903.
56. Schreiber T. Measuring information transfer. Phys Rev Lett 2000;85(2):461–464. [PubMed: 10991308]
57. Mormann F, Lehnertz K, David P, Elger CE. Mean phase-coherence as a measure for phase synchronization and its application to the EEG of epilepsy patients. Physica D 2000;144(3–4):358–369.
58. Lachaux JP, Rodriguez E, Martinerie J, Varela FJ. Measuring phase synchrony in brain signals. Hum Brain Mapp 1999;8:194–208. [PubMed: 10619414]
59. Sameshima K, Baccala LA. Using partial directed coherence to describe neuronal ensemble interactions. J Neurosci Meth 1999;15:93–103.

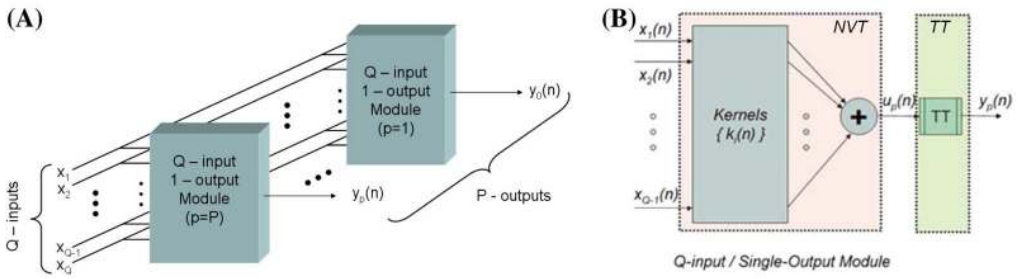

Fig. 1.

(A) Schematic representation of the decomposition of the MIMO model into an array of MISO modules. (B) Schematic detail of the structure of the MISO module comprising the cascade of the NVT and the TT operators.

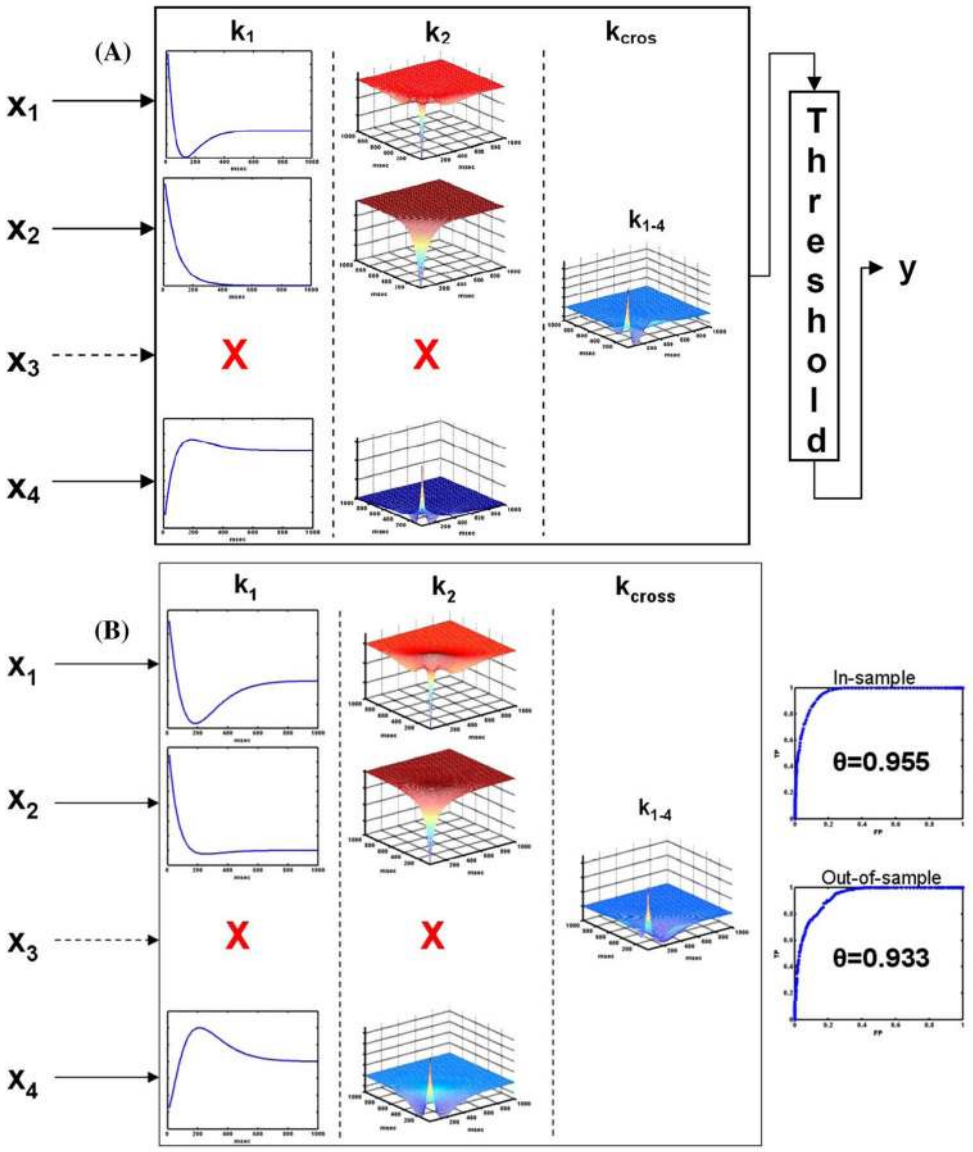

Fig. 2.

(A) Kernels of the second-order simulated MISO system with four inputs and one output: the first column shows the first-order kernels, the second column shows the second-order self-kernels, and the third column shows the cross-kernel between the first and the fourth input (see text). (B) The estimated kernels of this second-order model from the simulated data for the noise free case, along with ROC curves and theta values of in-sample and out-of-sample prediction (see text). The *x* axes in the first-order kernels and the *x* and *y* axes in the second-order kernels range from 0 to 1000 ms, while the ROC curves have in both axes values from 0 to 1.

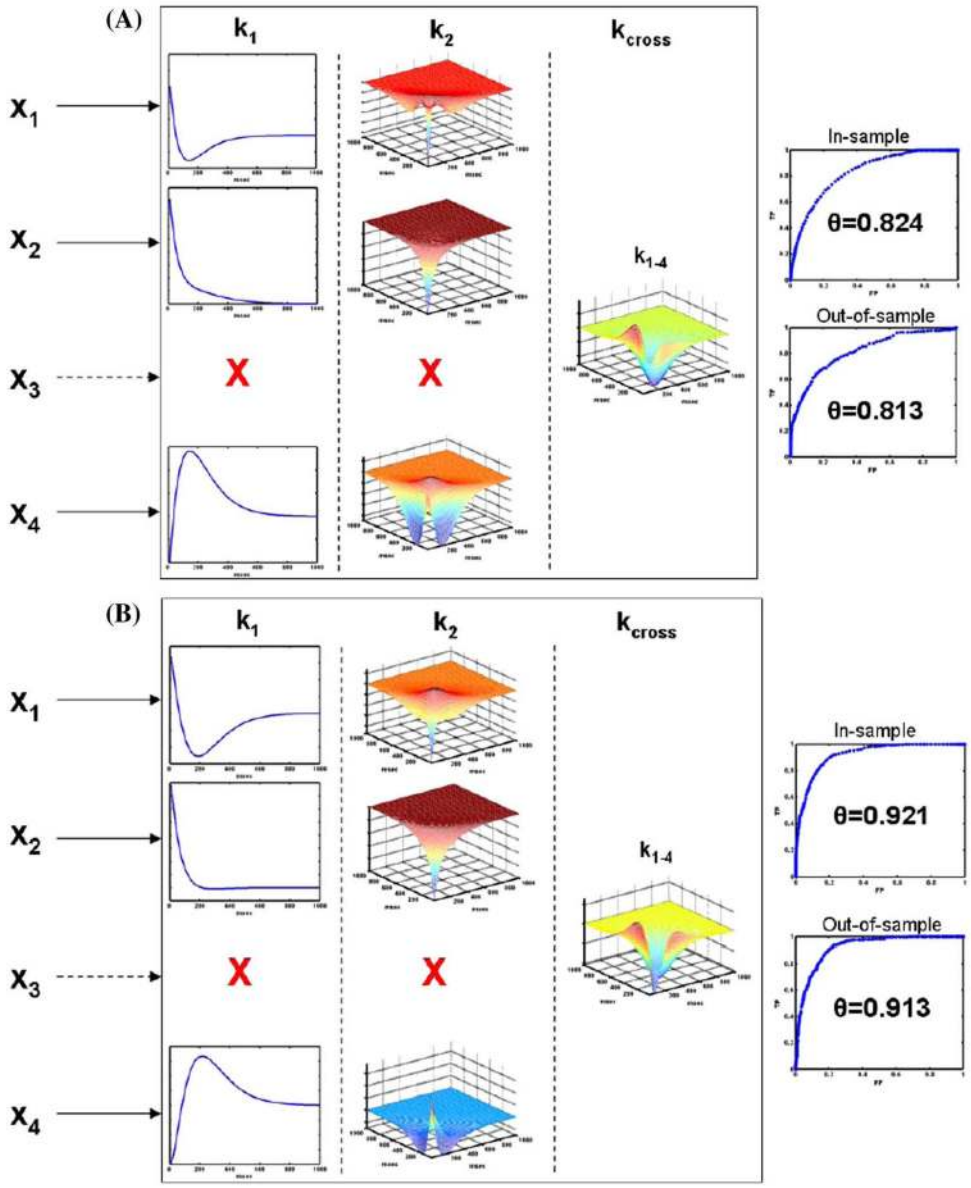

Fig. 3.

(A) The estimated model for the case of 50% spurious spikes in the inputs and output and (B) for the case of jitter in the spike location in the input–output data (see caption of Fig. 2 for detailed description of the layout and the axes of the plots). The results demonstrate the robustness of the proposed methodology in the presence of added spurious spikes and jitter.

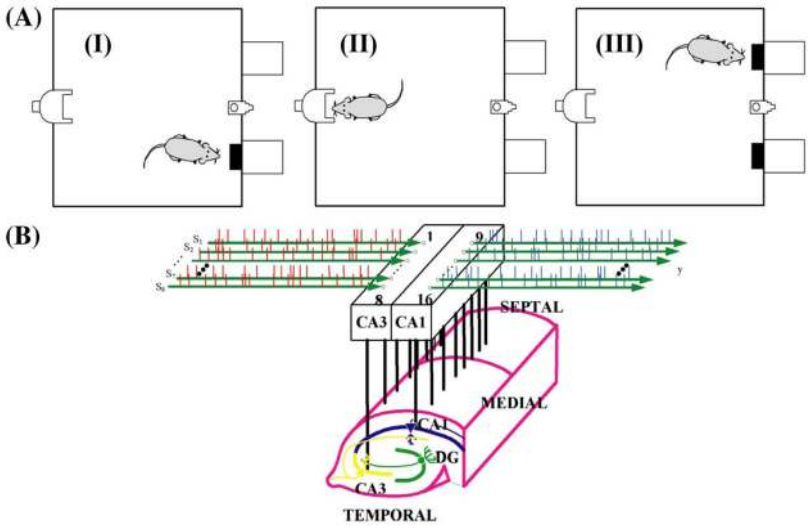

Fig. 4.

Schematic of the three behavioral tasks that the live rat is performing in each trial of the experiment: (I) right sample, (II) delay phase, (III) left nonmatch. (B) Schematic representation of the multielectrode array stimulating and recording arrangement in the CA3 and CA1 hippocampal regions of the behaving rat.

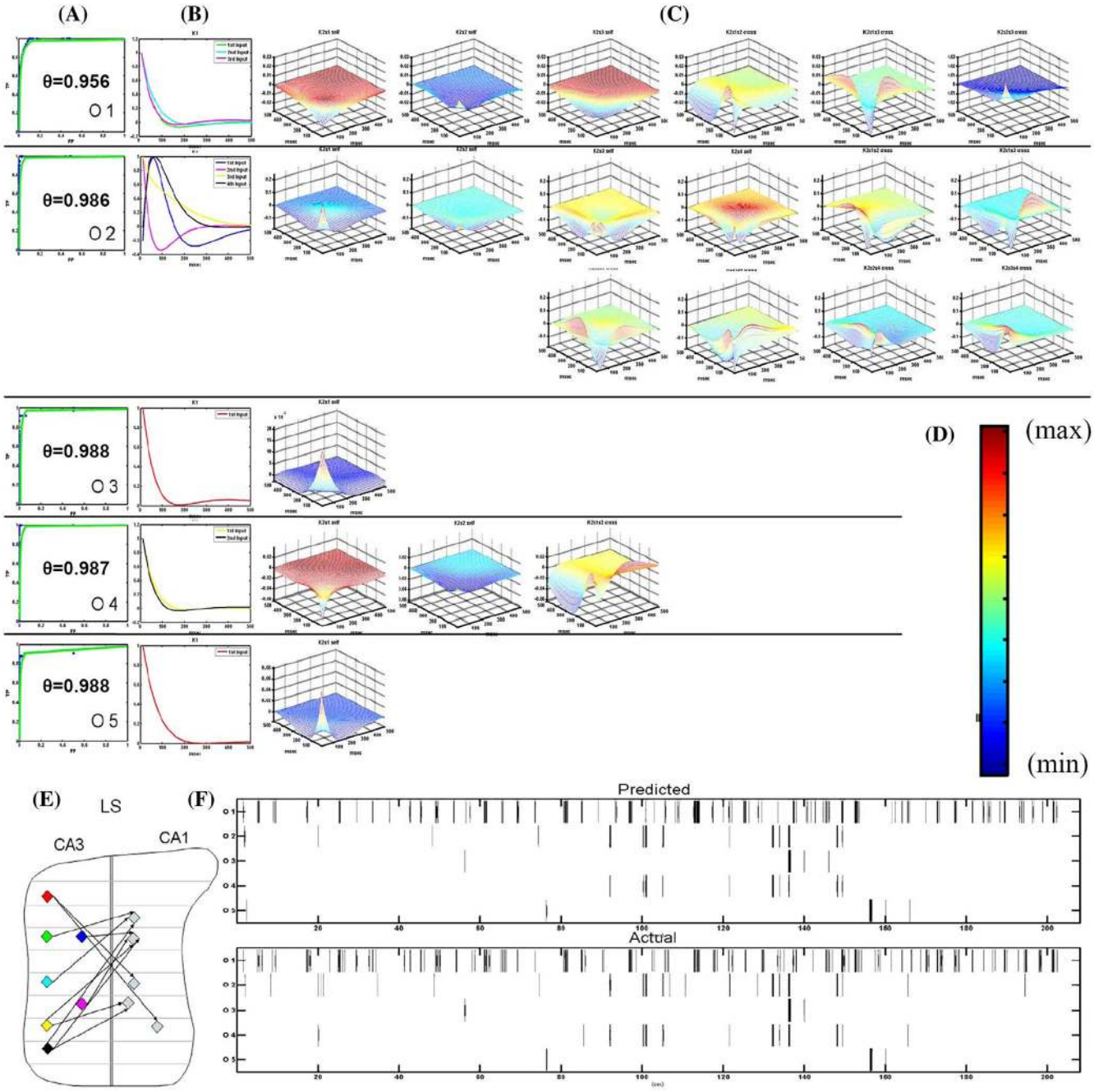

Fig. 5.

Illustrative Case of a complete MIMO model for the left sample event. (A) ROC curve and theta estimate of each output, (B) first-order kernels, (C) second-order self-kernels and cross-kernels, (D) colormap of the meshes used for the second-order kernels, (E) schematic of the topology of the input–output neurons in the CA3 and the CA1, respectively, and the causal connections considered in the MIMO model, (F) the model prediction and the actual recorded activity of each output neurons during the left sample task). The *x* axes in the first-order kernels and the *x* and *y* axes in the second-order kernels range from 0 to 500 ms, while the ROC curves have in both axes, values from 0 to 1.

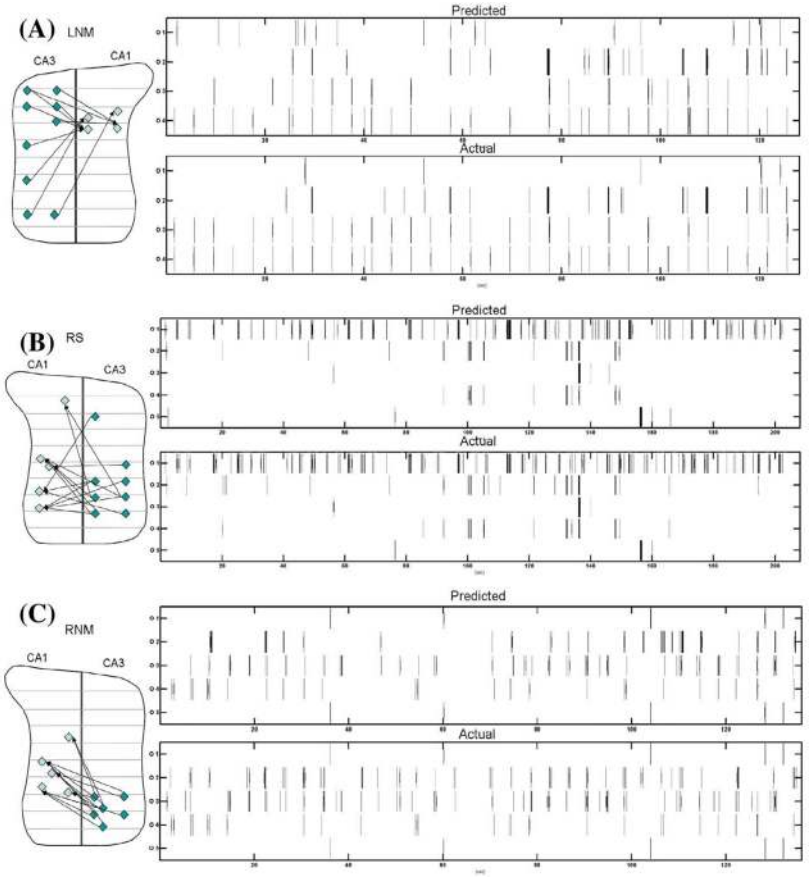

Fig. 6.

Schematic of the topology of the input–output neurons in the CA3 and the CA1, respectively, and the causal connections considered in each model (left panels). The model predicted and the actual recorded activity of the output neurons during three behavioral tasks: (A) left nonmatch, (B) right sample, and (C) right nonmatch. The time axes in all the prediction plots are in seconds.

TABLE I

Results of MWS-Based Test For Input Significance in the Simulated Noise-Free Case

Input	Estimated θ	95% cutoff value	Input Significant
x_1	0.833	0.565	Yes
x_2	0.752	0.561	Yes
x_3	0.545	0.563	No
x_4	0.723	0.573	Yes

TABLE II

Results of MWS-Based Test for Input Significance in the Simulated 25% Added Noise Case

Input	Estimated θ	95% cutoff value	Input Significant
x_1	0.829	0.558	Yes
x_2	0.758	0.564	Yes
x_3	0.549	0.566	No
x_4	0.705	0.568	Yes

TABLE III

Results of MWS-Based Test for Input Significance in the Simulated 50% Added Noise Case

Input	Estimated θ	95% cutoff value	Input Significant
x_1	0.684	0.556	Yes
x_2	0.611	0.553	Yes
x_3	0.528	0.56	No
x_4	0.632	0.554	Yes

TABLE IV

Results of MWS-Based Test for Input Significance in the Simulated Jitter Case

Input	Estimated θ	95% cutoff value	Input Significant
x_1	0.8	0.574	Yes
x_2	0.64	0.575	Yes
x_3	0.562	0.575	No
x_4	0.69	0.574	Yes

TABLE V

Results of MWS-Based Test for Input Significance in the Simulated Deleted Spikes Case

Input	Estimated θ	95% cutoff value	Input Significant
x_1	0.744	0.579	Yes
x_2	0.64	0.578	Yes
x_3	0.534	0.585	No
x_4	0.66	0.590	Yes

TABLE VI

Results of MWS-Based Test for Input Significance in the Simulated Misassigned Spikes Case

Input	Estimated θ	95% cutoff value	Input Significant
x_1	0.785	0.564	Yes
x_2	0.7	0.567	Yes
x_3	0.551	0.569	No
x_4	0.713	0.57	Yes

TABLE VII

Results of MWS-Based Test for Model Order Selection

Order	Estimated θ (var{θ})	p-value of t-test	Increase of Model Order Significant
1st	0.868(0.001)	-	-
2nd	0.961 (0.004)	0	Yes
3rd	0.82 (0.002)	1	No

TABLE VIII

Results of MWS-Based Test for Number of Laguerre Functions Selection

# of Laguerre Functions	Estimated θ (var{θ})	p-value of t-test	Increase of Laguerre Functions Significant
2	0.92 (0.007)	-	-
3	0.97 (0.003)	0	Yes
4	0.973 (0.003)	0.015	No

TABLE IX

Input Selection for the Four Behavioral Tasks

Input Selection for Left Sample Task			
Output Channel	**Input Channel(s)**	**Estimated θ**	**95% cutoff value**
39	9, 17, 29	0.698, 0.827, 0.804	0.580, 0.585, 0.579
41	10,22, 25,29	0.643, 0.666, 0.639, 0.637	0.629, 0.635, 0.628, 0.633
49	3	0.885	0.773
53	25,29	0.869, 0.878	0.701, 0.714
58	3	0.801	0.721
Input Selection for Left Non-Match Task			
Output Channel	**Input Channel(s)**	**Estimated θ**	**95% cutoff value**
38	31	0.883	0.777
39	17, 29	0.827, 0.804	0.662, 0.664
41	1, 3, 4,9	0.640, 0.560, 0.557, 0.766	0.583, 0.556, 0.554, 0.598
42	1, 2, 6	0.994, 0.720, 0.624	0.629, 0.632, 0.621
Input Selection for Right Sample Task			
Output Channel	**Input Channel(s)**	**Estimated θ**	**95% cutoff value**
66	121, 122	0.641, 0.760	0.639, 0.656
79	121, 122, 125	0.612, 0.954, 0.740	0.609, 0.616, 0.613
81	114, 125	0.669, 0.630	0.621, 0.619
87	101, 117, 126	0.597, 0.636, 0.645	0.568, 0.561, 0.569
91	117, 118, 122, 125	0.627, 0.657, 0.604, 0.615	0.563,0.563, 0.563, 0.563
Input Selection for Right Non-Match Task			
Output Channel	**Input Channel(s)**	**Estimated θ**	**95% cutoff value**
76	121, 122	0.957, 0.956	0.788, 0.781
81	122, 123, 125, 127	0.901, 0.588, 0.604, 0.562	0.561, 0.569, 0.568, 0.560
83	122, 123	0.900, 0.633	0.611, 0.598
85	123, 125, 126, 127	0.822, 0.695, 0.765, 0.696	0.685, 0.684, 0.688, 0.688
88	121, 123	0.999, 0.998	0.833, 0.849

TABLE X

Mann–Whitney Statistics for Final MIMO Model for LNM, RNM, and RS Tasks

Left Non Match Task			**Right Non Match Task**		
Output Channel	**Input Channels**	**θ**	**Output Channel**	**Input Channels**	**θ**
38	31	0.799	66	121, 122	0.984
39	17, 29	0.974	79	121, 122, 125	0.998
41	1, 3, 4, 9	0.913	81	114, 125	0.807
42	1, 2, 6	0.971	87	101, 117, 126	0.845
			91	117, 118,122, 125	0.807
Right Sample Task					
Output Channel			**Input Channels**	**θ**	
76			121, 122	0.946	
81			122, 123, 125, 127	0.639	
83			122, 123	0.944	
85			123, 125, 126, 127	0.949	
88			121, 123	0.951	

TABLE XI

Averaged Mann–Whitney Statistics for MISO Models Estimated From Randomly Generated Independent Poisson Spike Trains for Different MFRs and Numbers of Inputs

Mean MFRs of Data r	**2 spikes/sec**	**10 spikes/sec**	**20 spikes/sec**
Number of Inputs N-1	**mean theta (std theta)**		
2	0.609 (0.019)	0.558 (0.01)	0.543 (0.007)
3	0.611 (0.022)	0.583 (0.011)	0.563 (0.009)
4	0.620 (0.022)	0.609 (0.01)	0.583 (0.007)